JOURNAL OF MATERIALS SCIENCE 33 (1998) 2985–3000

Influence of short glass fibres and weldlines on the mechanical properties of injection-moulded acrylonitrile–styrene–acrylate copolymer

Z. U. NABI, S. HASHEMI
School of Polymer Technology, University of North London, Holloway Road, London N7 8DB, UK
E-mail: s.hashemi@unl.ac.uk.

The present study investigated the dependence of various mechanical and fracture properties on the volume fraction, ϕ_f, of reinforcing glass fibres in acrylonitrile–styrene–acrylate (ASA) copolymer. The addition of glass fibres enhanced the ultimate strength and modulus as measured in both tension and flexure but reduced the total work of fracture. The elastic modulus was not affected by the loading mode. The ultimate strength in flexure was found to be always greater than in tension by a factor of about 1.3. Both properties were found to be a linear function of ϕ_f following the rule of mixtures:

$$P_c = \lambda P_f \phi_f + P_m (1 - \phi_f)$$

where P_c is the measured property for the composite, P_f and P_m are the corresponding values for the fibre and the matrix, respectively, and λ is the overall efficiency of the reinforcing fibres. Addition of glass fibres to ASA polymer reduced both the notched and the unnotched impact strengths. Linear elastic fracture mechanics were used to determine values of the fracture toughness and the strain energy release rate. The fracture toughness did not change significantly with ϕ_f, whereas the strain energy release rate decreased with increasing ϕ_f. The presence of weldlines in the specimens had an adverse effect on all tensile properties except for the elastic modulus. The weldline integrity parameter for the modulus was between 1 and 0.95, and for strength it was between 0.87 and 0.20, decreasing linearly with increasing ϕ_f.

1. Introduction

It is common practice to lower costs and to improve mechanical properties of thermoplastics by incorporating fillers. In particular, the reinforcement of thermoplastics by short fibres has received special attention because of their use in a variety of engineering applications. In general, the stiffness and strength of the polymer matrix are enhanced by the addition of the short fibres. It has been shown [1–8] that the dependence of most mechanical properties on the volume fraction of the fibres can be described using some modified form of the rule of mixtures, which considers effects arising from both the orientation of the fibres and the distribution of fibre lengths through the injection-moulded component.

As most short-fibre composites are fabricated by injection moulding, it is desirable to determine the effect of weldline on mechanical properties. In polymer processing the term "weldline" is used to designate the interface created when two polymer melt fronts are brought into contact. Weldlines can be seen on the finished part as thin hair-like cracks on the surface. The local mechanical properties could be much lower in the weldline than in the bulk of the part, particularly in the short-fibre composites where fibres at the weldline may assume an orientation which is perpendicular to the direction of the applied stress.

The material chosen for the present work is acrylonitrile–styrene–acrylate (ASA) copolymer filled with six levels of glass fibre concentration ranging from 2 to 18 vol%. Deformation behaviour of the ASA and its composites was studied by a series of tensile and flexural tests. Fracture studies involved testing single-edge-notched bend (SENB) specimens in the three-point bend configuration. Moreover, since the influence of loading rate on material performance is an important consideration in material selection, deformation and fracture studies were performed by varying the loading rates. In addition, the influence of weldlines on tensile properties was also investigated.

2. Materials

ASA polymer under the tradename Luran S was supplied by BASF as the matrix material. This material is

made by the copolymerization of styrene and acrylonitrile (SAN) in combination with a grafted acrylic ester elastomer. The elastomer is in the form of very finely divided particles uniformly distributed in the SAN framework and bonded to it by grafted SAN chains. Short glass fibres of nominal length 6 mm and diameter 10 μm, coated with silane coupling agent, were used as a filler material.

3. Compounding

The polymer matrix was mixed with various amounts of short glass fibres to produce six composites with nominal glass fibre contents of 5, 10, 15, 20, 30 and 40 wt%. Compounding was carried out in a twin-screw extruder (Brabender) fitted with a die of diameter 4 mm. The melt temperature was kept constant at 270 °C and the screw speed was 12 rev min^{-1}. The extrudate strands were subsequently cooled and chopped into reinforced pellets and then dried in a vented oven at 70 °C for 3–4 h before injection moulding.

4. Mouldings

Two types of test specimen were injection moulded (Fig. 1).

(i) *Tensile bars*. Dumbbell-shaped specimens of dimensions 1.7 mm × 12.5 mm × 125 mm were produced on a Negri Bossi NB60 with a melt temperature of 270 °C and mould temperature of 70 °C. The mould used consisted of two cavities, a single- and a double-feed cavity in which the two opposing melt fronts meet to form a weldline midway along the gauge length.

(ii) *Flexural bars*. Flexural specimens of dimensions 120 mm × 10 mm × 4 mm were moulded using a Klockner Ferromatik F60 injection-moulding machine. The processing temperature was 270 °C and the mould temperature was 70 °C.

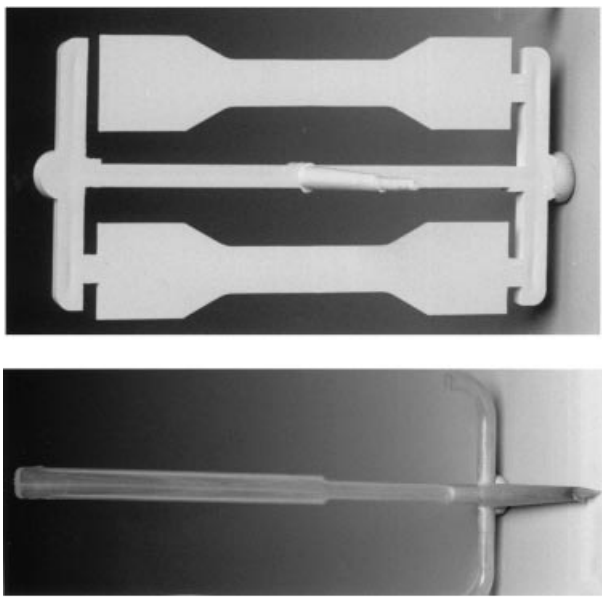

Figure 1 Tensile and flexural bars.

5. Sample characterization

5.1. Fibre concentration measurements

The fibre concentration in each composite was determined by ashing the material. Firstly it was necessary to determine the mineral content of the ASA matrix itself. A suitable amount of ASA polymer was weighed accurately and then placed in a furnace at 550 °C for at least 1 h. After cooling, the remnant was reweighed and the mineral filler content of the ASA polymer was calculated from the weight difference. The same ashing experiment was carried out with the injection-moulded fibre-reinforced ASA composites. The weight after ashing is the combined weight of the glass fibre and the mineral fillers in the ASA polymer. From a knowledge of the fibre and matrix densities, the volume fraction, ϕ_f, of the fibres was calculated from the weight fraction, w_f, of the fibres using the equation

$$\phi_f = \left[1 + \frac{\rho_f}{\rho_m}\left(\frac{1}{w_f} - 1\right)\right]^{-1}, \quad (1)$$

where ρ_m is the density of the matrix (1.07 g cm^{-3}) and ρ_f is the density of the glass fibre (2.54 g cm^{-3}). ϕ_f values are given in Table I.

5.2. Fibre length measurements

The same ashing experiment was carried out with the injection-moulded specimens in order to determine the average length of the fibre in each composite. The ash which contained a small quantity of mineral filler was examined under an optical light microscope. The fibre sample (from the remnant) was spread on a glass slide and then placed under a light microscope and photographed. At least 350 fibre lengths were measured and a frequency distribution of the fibre lengths for each composite was plotted as shown in Fig. 2. In a similar way as polymer chemists describe molecular weight distributions, we described the fibre length in terms of moments of distribution [8]:

$$L_n = \sum_i N_i L_i / \sum_i N_i \quad (2)$$

and

$$L_w = \sum_i N_i L_i^2 / \sum_i N_i L_i \quad (3)$$

where L_n and L_w represent number-averaged and weight-averaged fibre lengths. The result is shown in Table I, where the ratio L_w/L_n represents the fibre length polydispersity. It can be seen that, as the fibre content increases, the length of the fibre in the

TABLE I Sample characterization

Composite	w_f (%)	ϕ_f (vol%)	n	L_n (μm)	L_w (μm)	L_w/L_n
B	4.70	2.10	391	350	421	1.21
C	9.44	4.40	385	338	388	1.15
D	13.74	6.60	386	284	346	1.22
E	18.51	9.20	359	247	307	1.24
F	26.18	13.1	395	226	266	1.18
G	34.46	18.6	357	174	217	1.25

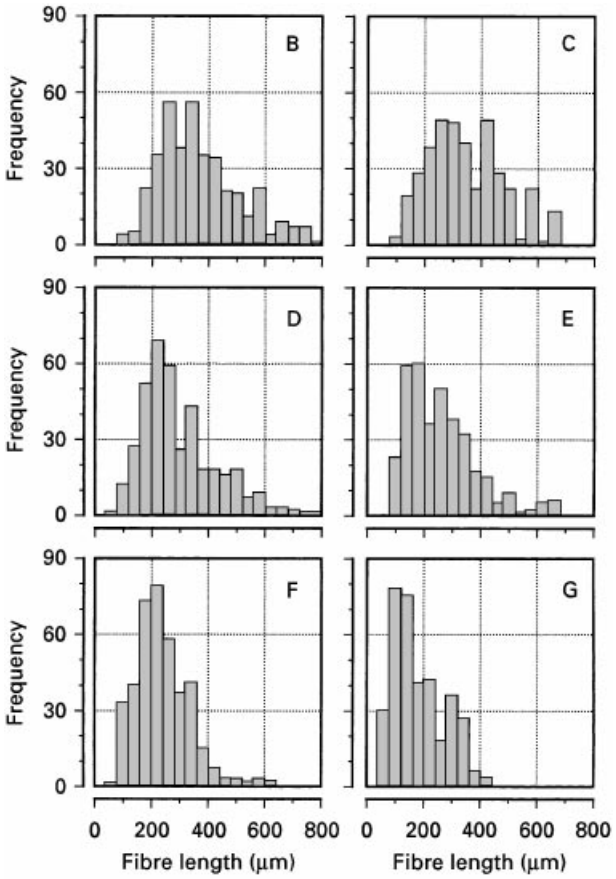

Figure 2 Fibre length distributions in ASA composite specimens.

composite decreases. This indicates that some degree of fibre degradation has taken place during compounding and moulding of the test specimens. The polydispersity showed no systematic variation with fibre content.

5.3. Fibre orientation

Surfaces of tensile and flexural bars to be examined were obtained by cutting the samples and polishing the sections. The polished sections were then viewed under an optical light microscope and photographed. Figs 3–5 are typical micrographs showing fibre orientation patterns in some selected unwelded and welded composite specimens as well as in the flexure bars (the flow direction is perpendicular to the plane of the paper).

6. Mechanical testing

6.1. Tensile tests

The tensile properties of the ASA polymer and its composites were measured in both tension and bending modes using an Instron testing machine.

Dumbbell specimens both with and without weldlines were tested in tension at cross-head displacement rates of 0.5, 5 and 50 mm min^{-1} using pneumatic clamps. Typical tensile load–displacement curves obtained from unwelded and welded specimens with various fibre concentration levels are reported in Figs 6 and 7, respectively.

6.2. Flexural tests

Measurements of flexural properties were made on flexural bars of dimensions 4 mm × 10 mm × 120 mm (depth × thickness × length). These tests were performed at a cross-head displacement rate of 5 mm min^{-1} over a span of 64 mm (i.e. span-to-depth ratio of 16 to 1). Typical load–displacement diagrams for some selected values of ϕ_f are shown in Fig. 8.

7. Dynamical mechanical analysis

Dynamic mechanical thermal analysis (DMTA) was carried out on strips 4 mm wide and 17 mm long, cut along the gauge length of the unwelded dumbbell specimens. Strips were tested in a three-point bend configuration with a span of 15 mm. All tests were performed in a Perkin–Elmer 7 series analyser at a frequency of 1 Hz, dynamic force of 400 mN and a static force of 600 mN. The temperature range over which testing was conducted was between 30 and 130 °C using increments of 2 °C min^{-1}. Typical traces of storage modulus for some selected values of ϕ_f are shown in Fig. 9.

8. Fracture toughness tests

Fracture tests for measuring fracture toughness and the material resistance to crack propagation were carried out on SENB specimens of dimensions width, $W = 10$ mm, thickness, $B = 4$ mm and length of 120 mm. For each material, a series of SENB specimens were prepared with the notch depth a, ranging from 2 to 7 mm. All the specimens were razor notched and tested to complete failure in three-point bending configuration with a 40 mm span. Cross-head displacement rates of 5 and 50 mm min^{-1} were used. Fig. 10 shows typical load–displacement curves for some selected composite specimens with different a/W ratios.

9. Impact tests

Notched and unnotched impact strengths as functions of glass fibre content were measured using three-point Charpy impact specimens of thickness, B, and depth, W, of 4 mm and 10 mm, respectively. Specimens were fractured at the pendulum speed of 3 m s^{-1} over a span of 40 mm. Notched impact tests were performed with an a/W ratio of 0.3 using a V-shaped notch with a tip radius of 0.25 mm.

10. Results and discussion

10.1. Microscopy

10.1.1. Unwelded tensile bars

The skin–core morphology which has been discussed by a number of workers (see, for example [9, 10]) was not found in these specimens. Instead, it was found that the cross-section of the unwelded tensile bars consists mainly of fibres whose long axes are oriented in the mould-fill direction (see Fig. 3). This orientation pattern was most obvious in the composite samples with higher fibre content.

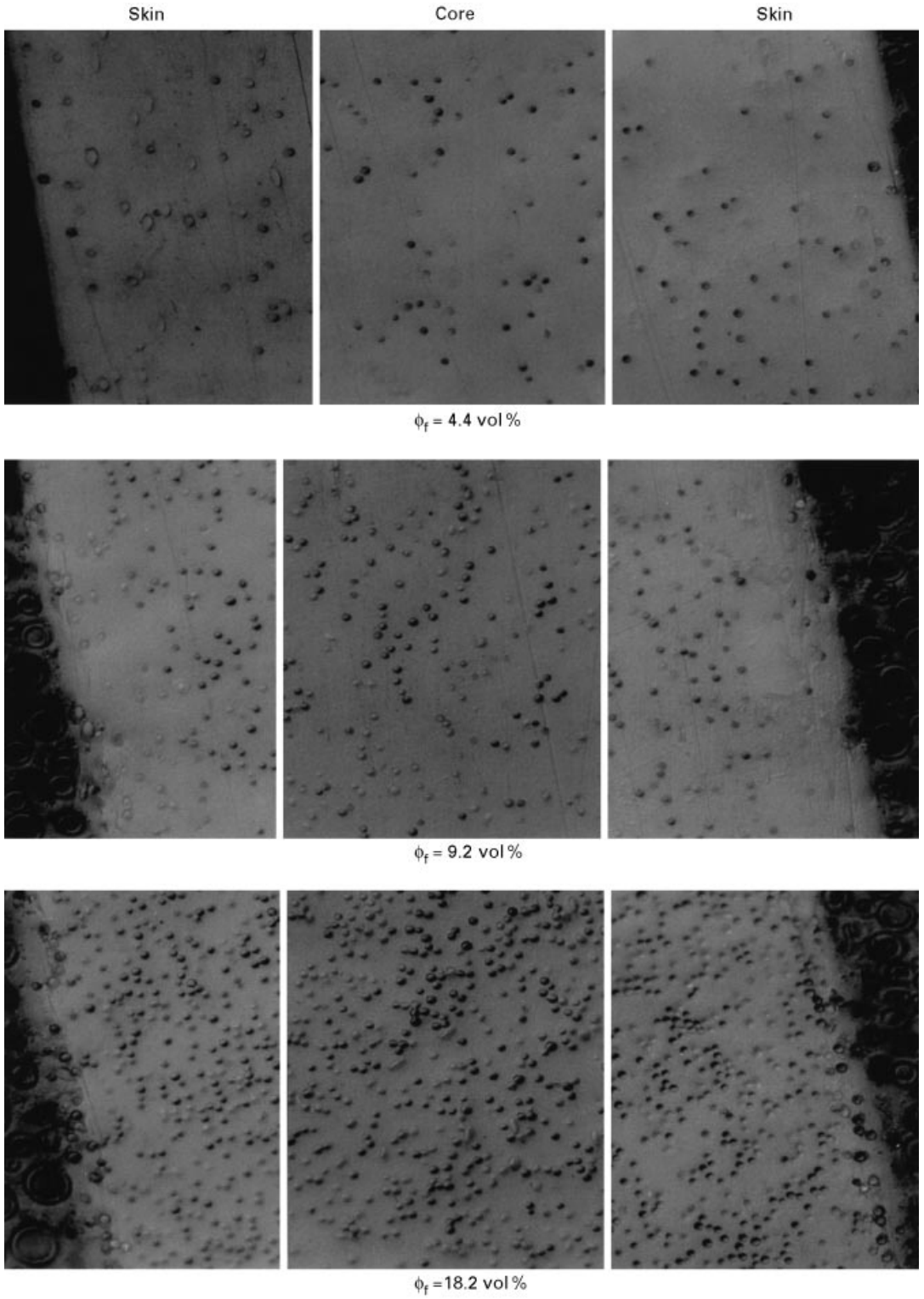

Figure 3 Optical micrographs showing the fibre orientation distribution through the thickness of the specimens without weldlines.

10.1.2. Weldline specimens

Fig. 4 shows the effect of fibre concentration on fibre orientation pattern through the thickness in the welded region. It can be seen that fibre orientation in the welded region consists mainly of fibres whose long axes are parallel to the weldline surface, i.e., perpendicular to the mould-fill direction. As one moves away from the weldline, fibre orientation changes and, at a distance of a few millimetres, the orientation pattern similar to that observed in the unwelded specimens is restored. This orientation pattern was most obvious in the composite samples with higher fibre content.

10.1.3. Flexural bars

Fig. 5 shows the effect of fibre concentration on fibre orientation pattern through the thickness of the flexural bars. Evidently, injection moulding of composite samples has led to the formation of a distinct core region sandwich between two surface skin layers. Surface "skin" layers consisted mainly of fibres whose

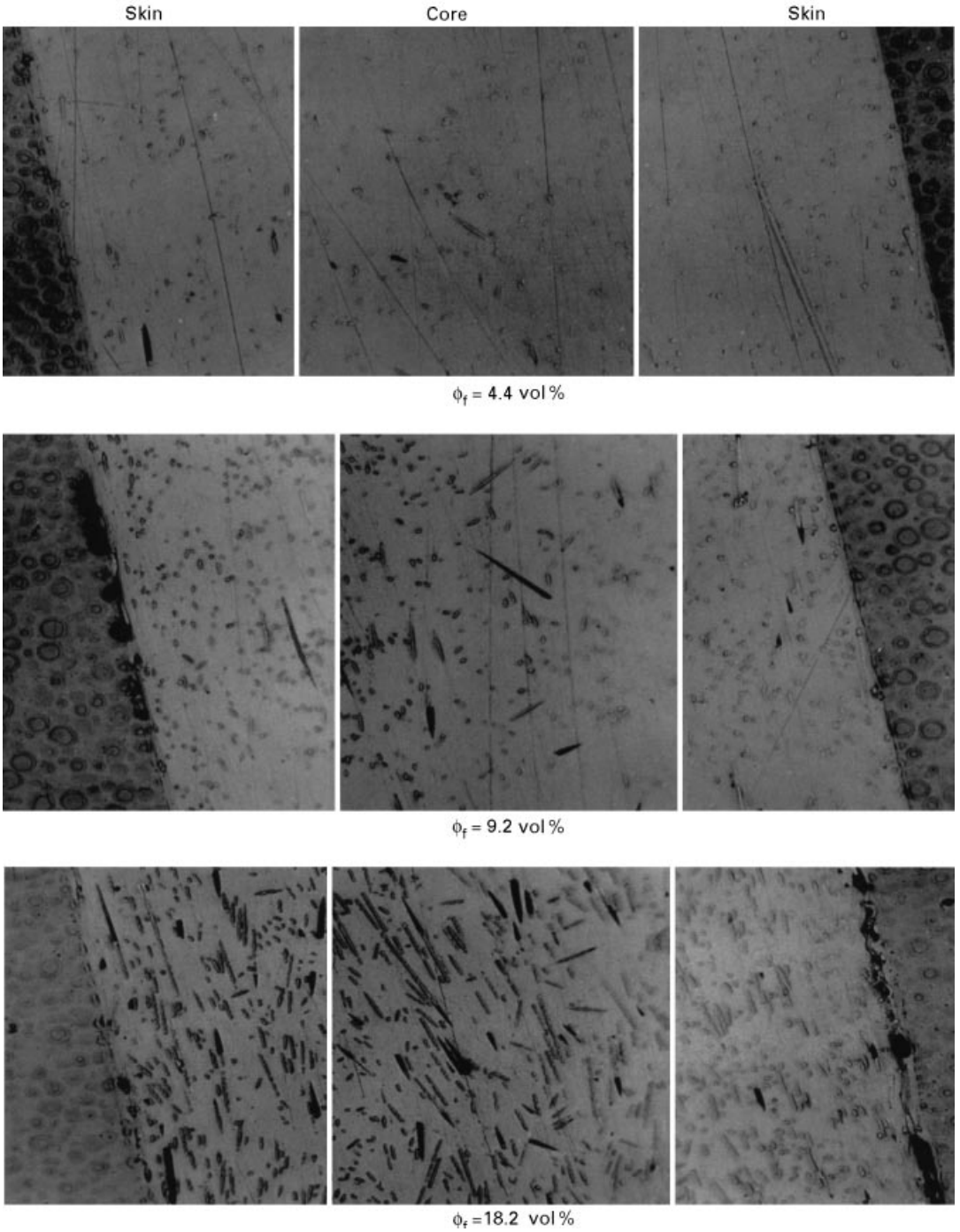

Figure 4 Optical micrographs showing the fibre orientation distribution through the thickness of the specimens with weldlines.

long axes were oriented in the mould-fill direction. The core region consisted of fibres that were randomly oriented. This morphology was most obvious in the composite samples with higher fibre content.

10.2. Elastic modulus

It is evident from the load–displacement diagrams that the addition of glass fibres to ASA has resulted in an increase in the initial slope of the load–displacement diagram. The initial slope was found to be more or less insensitive to the rate at which specimens were tensile tested. However, as illustrated in Fig. 11, values of the tensile modulus were found to be consistently lower than those of the flexural modulus. The difference between the two values widened as the volume fraction of glass fibres was increased. Since the modulus of the unfilled ASA was also lower in tension than in flexure, the difference between the two values could not be explained solely in terms of differences in fibre orientation patterns in the two types of specimen. As measured tensile values were based on the clamp separation, a follow-up study was done in which the gauge length of the tensile specimens was varied. This was done in an attempt to correct the tensile modulus for effects arising from machine compliance, clamps and gear train, all of which could lead to erroneous tensile results. These effects were brought together by the following relationship, which is based on the assumption of additivity of strains in the sample and the

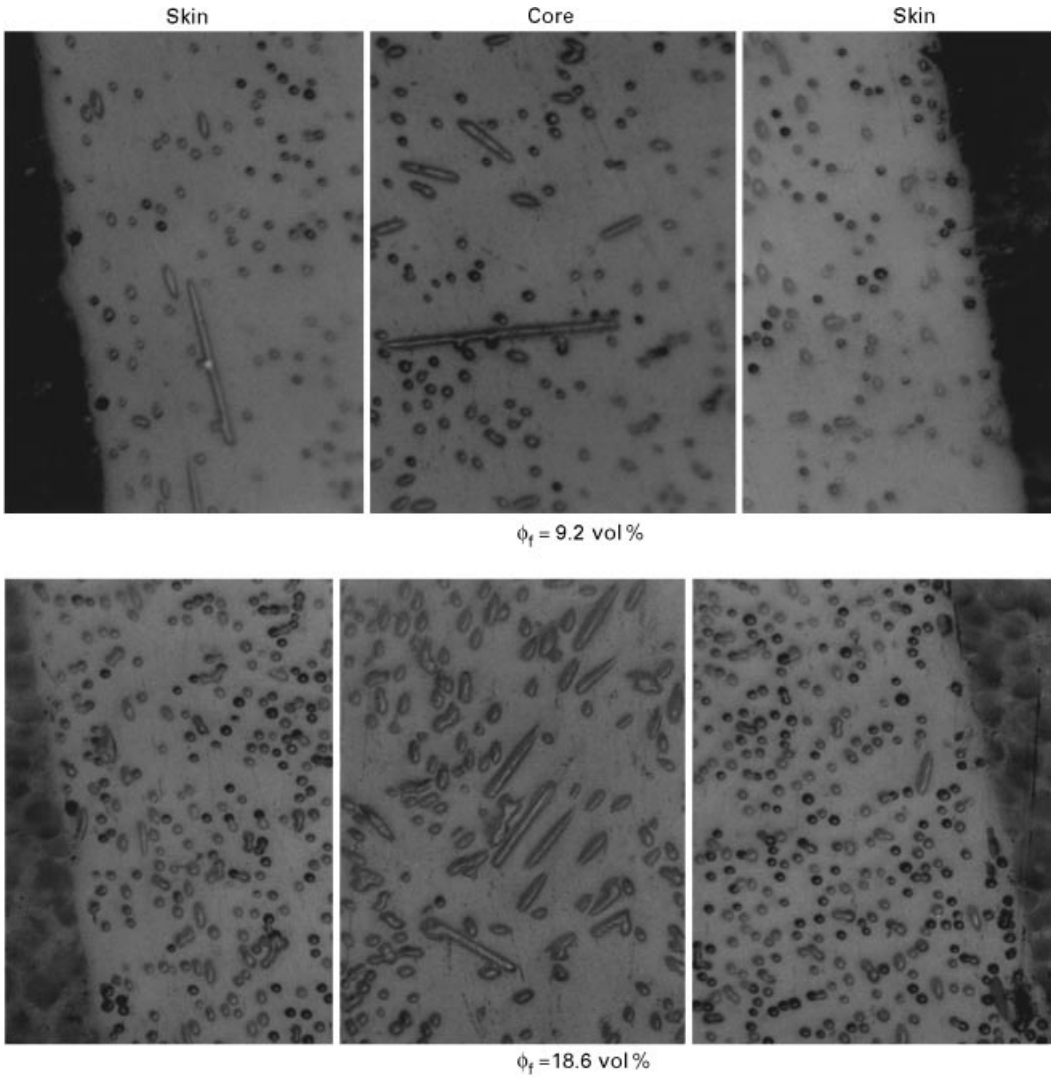

Figure 5 Optical micrographs showing the fibre orientation distribution through the thickness of flexural bars.

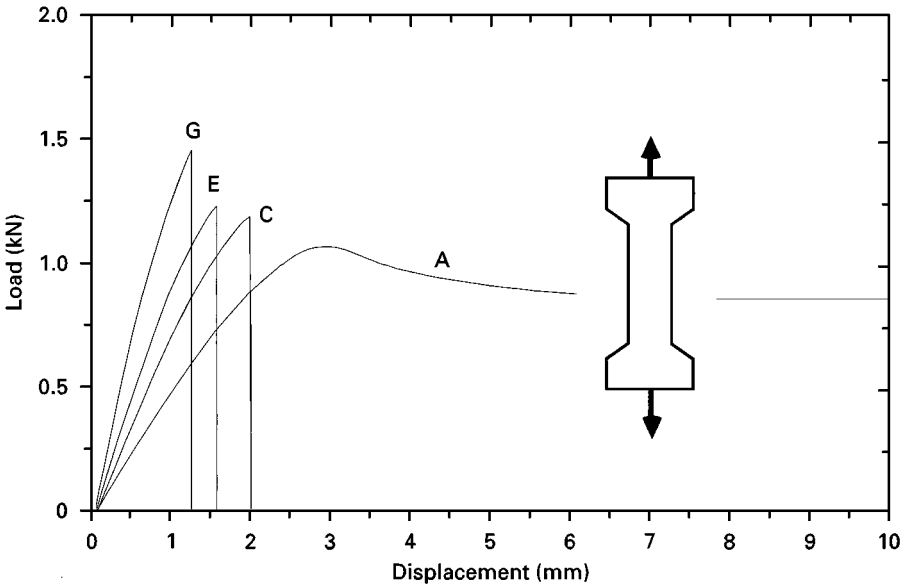

Figure 6 Tensile load–displacement traces for some selected specimens without weldlines.

instrument:

$$\frac{1}{E_{app}} = \frac{1}{E_{act}} + k\frac{A}{Z} \quad (4)$$

where E_{app} is the apparent Young's modulus (with no correction being applied), E_{act} is the actual Young's modulus, k represents the instrument constant, and A and Z are the cross-sectional area and the gauge

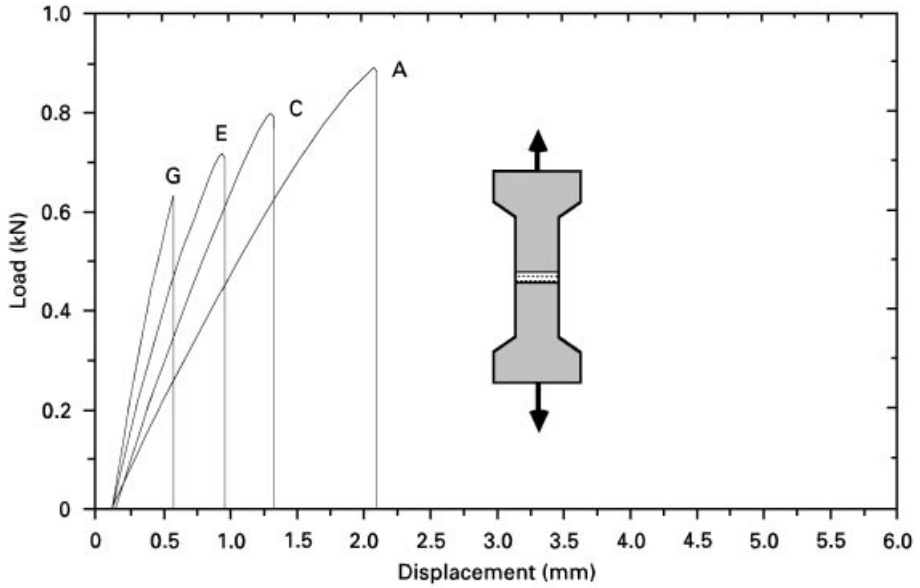

Figure 7 Tensile load–displacement traces for some selected specimens with weldlines.

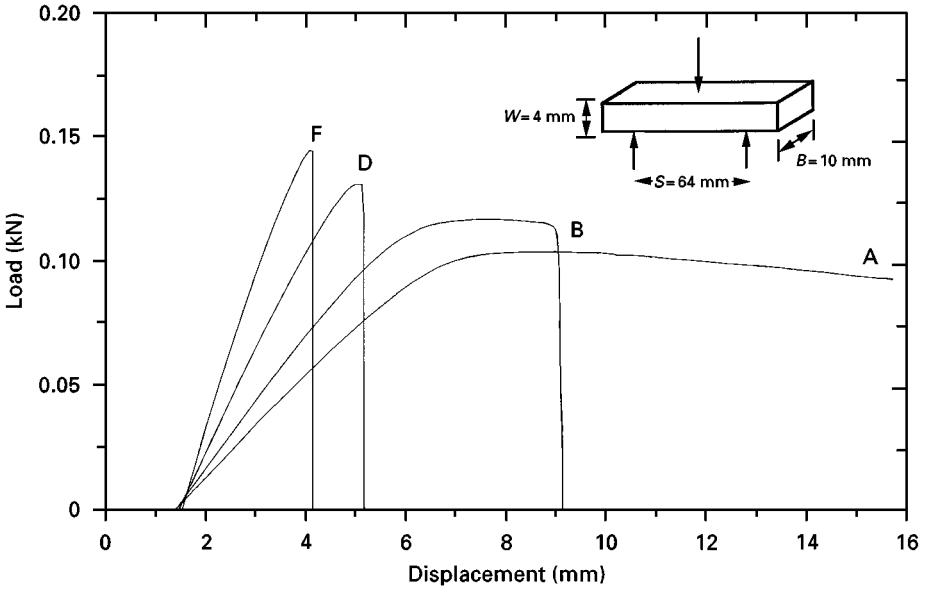

Figure 8 Flexural load–displacement traces for some selected materials.

length, respectively, of the test specimen. According to Equation 4, E_{act} can be evaluated by linearly interpolating the plot of $1/E_{app}$ versus A/Z. The inverse of the intercept at $A/Z = 0$ is E_{act} and the slope of the line is k. Such a plot for both unfilled and filled ASA polymer is shown in Fig. 12, where it can be seen that the data agree reasonably well with Equation 4. As indicated in Fig. 11, the corrected values of tensile modulus are significantly higher than those of uncorrected values. Moreover, the corrected values appear to agree reasonably well with modulus values determined in flexure. This confirms our earlier belief that the difference between the tensile and flexural moduli did not arise as a result of a fibre orientation effect but was the manifestation of machine compliance and so forth.

The linear dependence between the elastic modulus, E_c, and ϕ_f (see Fig. 11) can be described reasonably well by the following equation (solid line in Fig. 11):

$$E_c = 2.29 + 32.31\phi_f \tag{5}$$

The simplest equation for the prediction of the elastic modulus of the short fibre composites is by the modified rule of mixtures [1–8]:

$$E_c = \lambda_1\lambda_2 E_f\phi_f + E_m(1 - \phi_f) \tag{6}$$

where E_f is the modulus of the fibre, E_m is the modulus of the matrix, and λ_1 and λ_2 are the fibre length and orientation efficiency factors, respectively, for the modulus. λ_1 considers the reinforcing effectiveness of the short fibres and its value can be estimated from

$$\lambda_1 = 1 - \frac{\tanh(\beta L/2)}{\beta L/2} \tag{7}$$

where L is the average length of the fibre and β is defined as

$$\beta = \left(\frac{\pi E_m}{E_f(1 + \nu_m) A_f \ln(R/r)} \right)^{1/2} \quad (8)$$

where ν_m is Poisson's ratio for the matrix, r is the radius of the fibre, R is the centre-to-centre distance of the fibres and A_f is the area of the fibre. For square packed fibres,

$$R = r\left(\frac{\pi}{4\phi_f} \right)^{1/2} \quad (9)$$

Equation 7 can be rearranged to give

$$E_c = E_m + (\lambda_E E_f - E_m)\phi_f \quad (10)$$

where $\lambda_E = \lambda_1 \lambda_2$, commonly known as the overall efficiency parameter for modulus.

Comparing Equations 5 and 10, we obtain an overall efficiency factor of 0.46 for the modulus (taking E_f as 75 GPa). Using this value and the λ_1 values calculated via Equation 7 (taking ν_m as 0.35 and r as 5 μm) we obtain λ_2 values between 0.62 and 0.68 as given in Table II. These relatively high values of λ_2 suggest that fibres in the two mouldings are aligned substantially in the mould-fill direction; similar values have been obtained from composites having different matrices [2, 6, 7] but processed using identical mouldings as in Fig. 1.

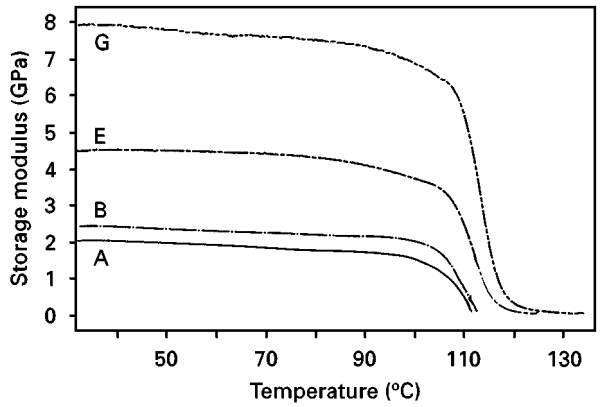

Figure 9 Typical DMTA traces for some selected materials.

10.2.1. Influence of weldline on elastic modulus

As regards weldlines and their influence on elastic modulus, we found that the deformation behaviour in the "elastic region" was only marginally affected by the presence of the weldline (see Fig. 7). The modulus retention ratio or the weldline integrity parameter as it is commonly known (the ratio of the modulus of a specimen with a weldline to that of the modulus of an equivalent specimen without a weldline) ranged between 1.0 and 0.95 for the range of ϕ_f values used here, thus implying that the elastic modulus is not very sensitive to weldlines. This behaviour was interpreted using the model shown in Fig. 13. The model predicts that the modulus, $\bar{E}$, of the welded specimen is related to the modulus, E_1, of the material outside the weldline and to the modulus, E_2, of the material inside the weldline by the following relationship:

$$\bar{E} = \frac{E_1 E_2}{E_2 + (E_1 - E_2)z} \quad (11)$$

However, since z is very small for these materials, the second term in the denominator is small compared with E_2, thus indicating the $\bar{E} \approx E_1$ as was observed in the present study.

10.3. Strength

10.3.1. Unwelded tensile behaviour

It is evident from the load–displacement diagrams shown in Fig. 6 that the matrix material shows lower

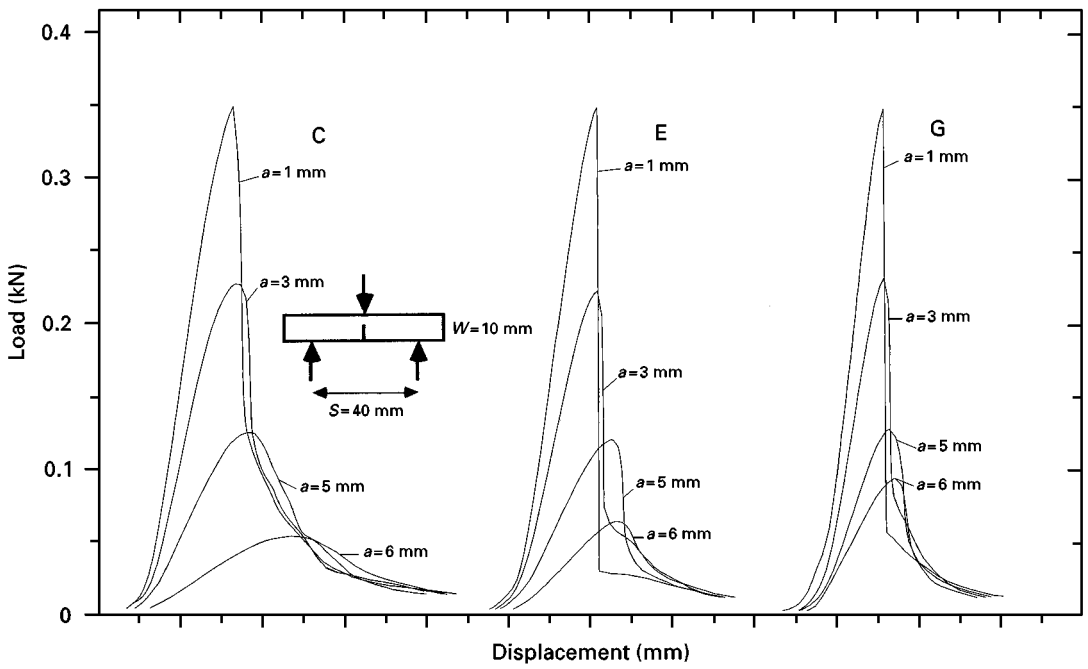

Figure 10 SENB load–displacement diagrams for some selected composites.

strength but higher extension to failure than its composites. This arises because the matrix material is confined by the fibres and therefore cannot deform freely. In a composite the matrix is subjected to a triaxial state of stress, even when a uniaxial stress is applied to the composite. The triaxial restraint of the matrix between the fibres limits the elongation of the matrix and therefore reduces its elongation to failure.

The dependence of the unwelded tensile strength on volume fraction of the glass fibres at various crosshead speeds is shown in Fig. 14. It can be seen that the overall trend for fibre concentration values between 0 and 13 vol% is that of increasing tensile strength with increasing fibre concentration. However, at a fibre concentration value of 19%, tensile strength tends to be lower than the trend. This is consistent with a previous study [11] where it was found that, at volume fractions close to 20%, the separation distance between the fibres could become sufficiently small to restrict the flow of matrix material. This effect, as well as the greater number of fibre ends, which leads to higher stress concentration in the matrix material, tend to reduce the gains in strength which otherwise would be expected at high fibre concentration values. Moreover, we should point out that some degree of surface roughness was observed during compounding of this grade, which may have also affected strength properties in addition to the aforementioned factors.

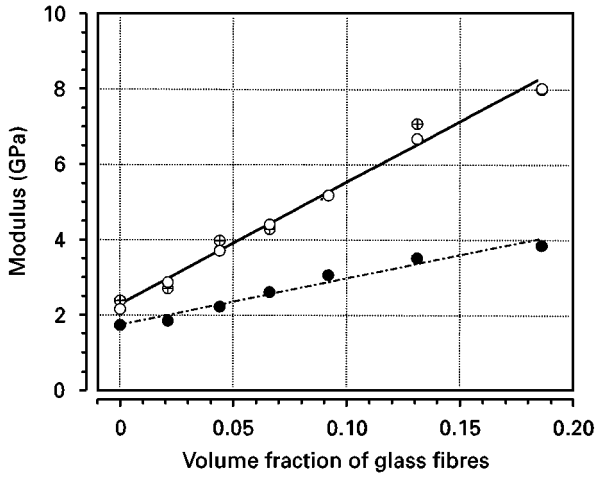

Figure 11 Tensile and flexural modulus versus volume fraction of glass fibres.

The linear dependence of tensile strength on ϕ_f as shown in Fig. 14 can be expressed as

$$\sigma_c = \sigma_0 + \alpha\phi_f \tag{12}$$

where the intercept value, σ_0 (at $\phi_f = 0$), and the slope, α, are both dependent on the rate of testing, the latter increasing and the former decreasing with increasing rate. The intercept values, σ_0, were within 2–5% of the matrix tensile yield strength values. According to Kelly and Tyson [1], the effect of fibre concentration on the composite strength may be predicted by the following rule of mixtures for strengths:

$$\sigma_c = \lambda_3\lambda_4\sigma_f\phi_f + \sigma_m(1 - \phi_f) \tag{13}$$

where σ_f and σ_m are the tensile strengths of the fibre and the matrix respectively. λ_3 represents contributions to the strength from the fibre length and λ_4 represents the contributions to the strength from the fibre alignment distribution. In a similar way to Equation

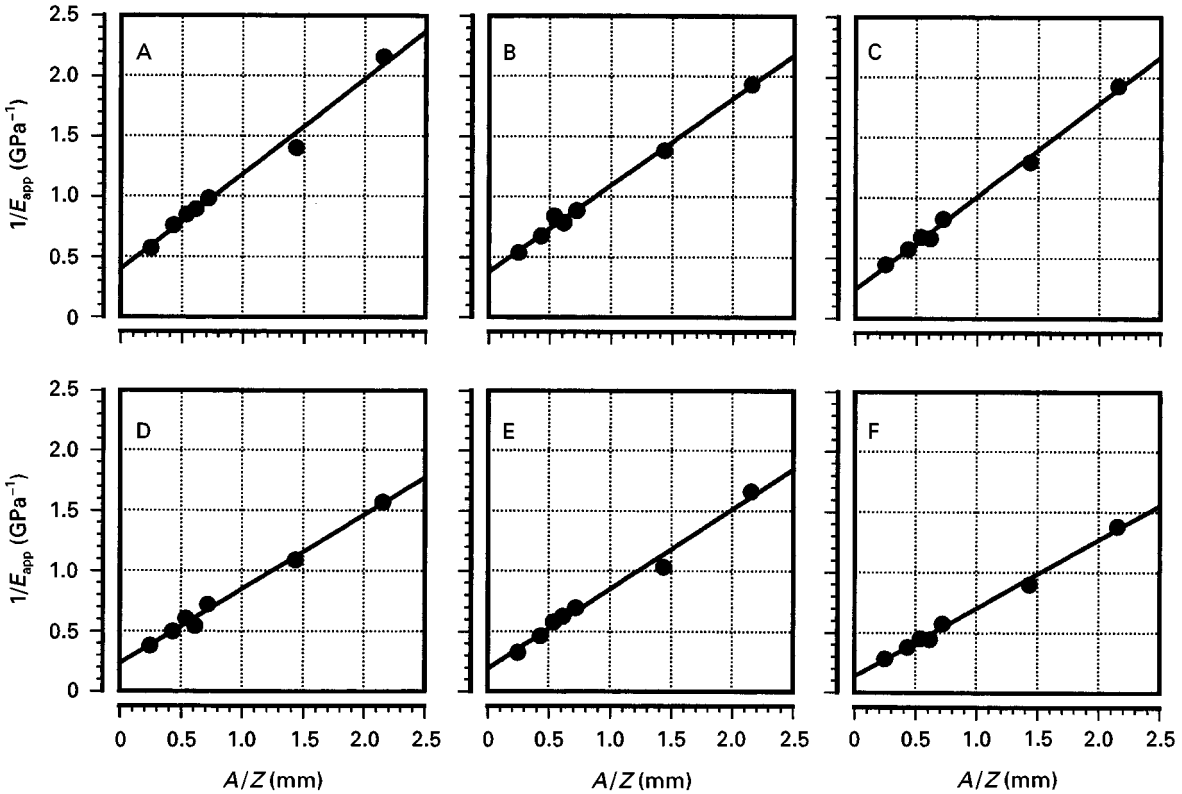

Figure 12 Apparent tensile modulus versus A/Z for the ASA and its composites.

TABLE II Efficiency parameters for modulus and strength

ϕ_f (vol%)	Modulus efficiency parameter ($\lambda_E = 0.46$)		Strength efficiency parameter ($\lambda_S = 0.081$)		τ_i(MPa) $\lambda_4 = \lambda_2 = 0.64$
	λ_1	λ_2	λ_3	λ_4	
2.1	0.75	0.62	0.34	0.24	8.96
4.4	0.76	0.61	0.32	0.25	9.28
6.6	0.74	0.62	0.27	0.30	11.05
9.2	0.72	0.64	0.24	0.34	12.70
13.1	0.72	0.64	0.22	0.38	13.88
18.6	0.68	0.68	0.17	0.49	18.03

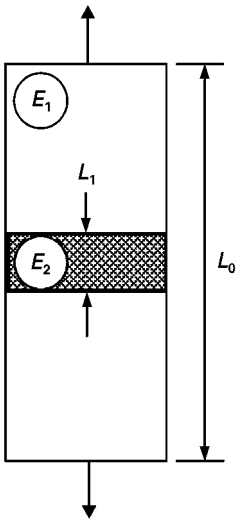

Figure 13 Model used for the prediction of the tensile modulus in welded specimens. The total deformation along the length of the sample is given by

$$\delta_T = \delta_1 + \delta_2$$

Assuming linear elastic deformation

$$\delta = eL = L\frac{\sigma}{E}$$

Substituting into $\delta_T = \delta_1 + \delta_2$ gives

$$\sigma\frac{L_0}{E} = \frac{\sigma_1 L_0(1-z)}{E_1} + \frac{\sigma_2 L_0 z}{E_2}$$

where $L_1 = zL_0$. Since $\sigma = \sigma_1 = \sigma_2$, hence

$$\frac{1}{E} = \frac{1-z}{E_1} + \frac{z}{E_2}$$

$$\frac{1}{E} = \frac{E_2(1-z) + E_1 z}{E_1 E_2}$$

Hence

$$E = \frac{E_1 E_2}{E_2 + (E_1 - E_2)z}.$$

10, we may write

$$\sigma_c = \sigma_m + (\lambda_S \sigma_f - \sigma_m)\phi_f \quad (14)$$

where λ_S is the overall efficiency parameter for strength ($\lambda_S = \lambda_3\lambda_4$). Comparing Equations 12 and 14 we see that the overall efficiency factor for strength is approximately 0.081 at all three rates (taking σ_f as 2470).

The efficiency of the fibre as a reinforcing filler depends on whether the average length is subcritical or supercritical. The critical fibre length, L_c, is defined as [1]

$$L_c = \frac{d\sigma_f}{2\tau_i} \quad (15)$$

where d is the fibre diameter and τ_i is the fibre matrix shear strength. The fibre length efficiency factor, λ_3, for strength for the case in which $L_n < L_c$ may be calculated from

$$\lambda_3 = \frac{L_n}{2L_c} \quad (16)$$

and for the case in which $L_n > L_c$ from

$$\lambda_3 = 1 - \frac{L_n}{2L_c} \quad (17)$$

Assuming that the shear strength of the interface is half the tensile yield strength of the matrix, we estimate that the critical fibre length is approximately 523 μm. Clearly, this value is greater than the average fibre lengths given in Table I; consequently, the values of λ_3 were calculated using Equation 16. These values are also given in Table II together with λ_4 values estimated using values of λ_E and λ_3.

It can be seen from Table II that, the values of the efficiency parameters, λ_E, λ_1 and λ_2, for the modulus are consistently higher than the values of the efficiency parameters, λ_S, λ_3 and λ_4, for strength. A particular concern is the large discrepancy between the two orientation efficiency parameters, λ_2 and λ_4, the former being approximately 2.5 times greater than the latter. This discrepancy, we believe, has originated from the overestimation of the interfacial shear strength which directly affects the λ_3 values. In our calculations we assumed that interfacial adhesion between the fibres and the matrix was reasonable and therefore assigned its value as half the matrix yield strength. There is, however, a clear indication, based on a λ_S value of 0.081, that interfacial adhesion is poor. This was further substantiated by scanning electron microscopy of the fracture surfaces which indicated that fibre surfaces were completely free from any polymer matrix. It must be noted that, since the yield stress value is measured at larger deformations, it is more dependent upon the interfacial adhesion than upon the elastic modulus, where measurements are restricted to very small deformations. This is why, for instance, the tensile yield stress is often used to correlate interfacial interactions in heterogeneous polymer systems [12]. Assuming that λ_4 values should not differ significantly from λ_2 values, we obtain that $\lambda_3 = 0.13$ (taking λ_2 as 0.64 and λ_S as 0.081). The estimated τ_i values thus range between 9 and 18 MPa as shown in Table II, increasing with increasing ϕ_f.

The dependence of the tensile strength on the rate of testing is shown in Fig. 15, where it can be seen that for a given ϕ_f value the general trend is that of increasing tensile strength with increasing rate owing to the brittleness of the polymer matrix. It is worth noting that, for a fixed value of ϕ_f, the relationship between the

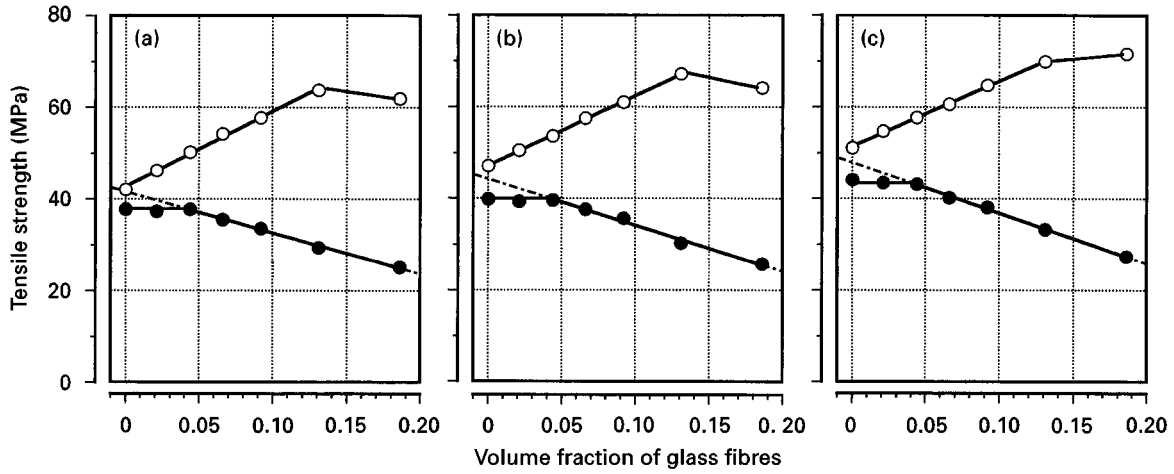

Figure 14 Welded (●) and unwelded (○) tensile strengths versus volume fraction of glass fibres at cross-head displacement rates of (a) 0.5 mm min^{-1}, (b) 5 mm min^{-1} and (c) 50 mm min^{-1}.

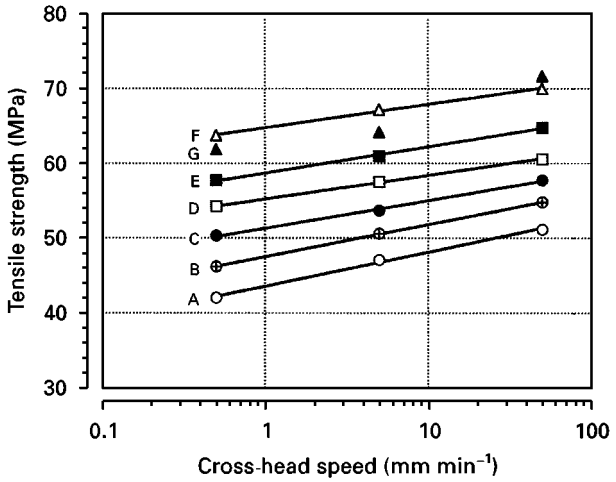

Figure 15 Unwelded tensile strength versus loading rate for ASA and its composites.

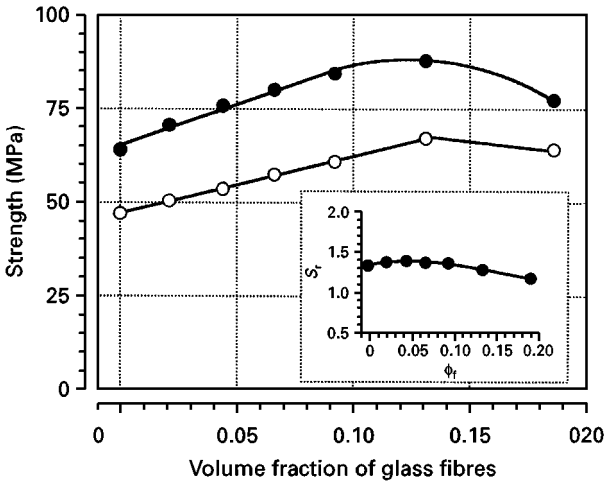

Figure 16 Comparison between tensile (○) and flexural (●) strength as functions of volume fraction of glass fibres.

tensile strength and the testing rate, x, can be reasonably described as

$$\sigma_c = K_1 + K_2 \log x \quad (18)$$

where K_2 decreases from a value of 4.56 for the matrix to a value of 3.12 for the sample containing 13 vol% glass fibres.

As for the dependence of flexural strength on fibre concentration, it can be seen from Fig. 16 that the trend is similar to that of the tensile strength. However, in line with previously reported results (see, for example, [2, 6, 7]), albeit on different composite systems, the flexural strengths appears to be consistently higher than the tensile strengths. The ratio, S_r, of the two strengths (inset in Fig. 16) showed little variation with respect to ϕ_f, particularly in the concentration range between 0 and 13 vol%, where the ratio is found to be between 1.31 and 1.40. It must be noted that the correction applied to the tensile modulus does not apply to the tensile strength, where one needs to know only the load and the area, but not the strain. It has been suggested that the difference between the two strengths is due to the differences in fibre orientation patterns in the two mouldings. We acknowledge that the presence of the core region in flexural bars and its absence in tensile bars, as observed here, may in part be responsible for higher flexural strengths. However, in view of the fact that the stress ratio for the unfilled matrix is not significantly different from that of the filled matrix, we believe that the differences arise mainly from the combination of the following factors.

(i) *A non-uniform stress distribution in bending as opposed to a uniform stress distribution in tension*: This implies that, in a tensile test, the whole volume of the specimen is subjected to the tensile state and thus the measured stress value is the mean value of the stress across the specimen thickness whereas, in bending, the maximum stress is reached only at the extreme tensile face of the specimen.

(ii) *Statistical aspect of fracture*. It has been observed by Weibull [13] that the strength of a brittle material is strongly dependent upon the volume and stress distribution and, because of this, the average maximum stress at failure in bending is expected to be higher than that of an identical specimen in tension since the number of flaws in the outer surface of the specimen is usually lower and their sizes smaller than in the bulk of the specimen.

(iii) *Cross-sectional yielding*: It is seen from Fig. 8 that the assumption of linear elastic deformation is not strictly valid as load–displacement diagrams clearly demonstrate that some degree of yielding has taken place in the cross-section of the flexural bars during bending. Such yielding could cause flexural strengths to be overestimated by a factor of as much as 1.5 if linear elastic analysis is used.

10.3.2. Influence of weldline on tensile strength

Failure of all weldline specimens was found to be brittle in nature (see Fig. 7). Beyond the elastic region the presence of the weldline resulted in a deviation of the load–displacement behaviour from that of the weld-free specimens. The effect of weldline on tensile strength is illustrated in Fig. 14. It is seen that tensile strengths of the filled and unfilled ASA are markedly reduced in the presence of weldlines. The strength loss for the unfilled ASA is due to the perpendicular-to-flow polymer chain orientation near the weldline region (i.e., perpendicular to the direction of the applied tensile force). As for the filled ASA, the strength loss is mainly due to the glass fibre orientation, and not to polymer chain orientation in the weldline region. As stated earlier, most glass fibres in the weldline region are oriented perpendicular to the direction of the melt flow which is also the direction of the tensile force. Thus, weldline specimens are expected to be weaker than weld-free specimens, where most fibres are oriented parallel to the tensile force direction.

It is seen also that the extent of deterioration in the weldline strength of the filled ASA depends largely on the concentration of the fibres in the specimen. Fig. 14 shows that up to a fibre concentration value of about 4.4 vol% there is virtually no change in weldline strength; however, above this value, the weldline strength decreases linearly with increasing ϕ_f. It may be deduced that, at low fibre concentration values (i.e., less than 4.4 vol%), the strength of the weldline is dictated mainly by the orientation of the polymer chains whereas, at high concentration values, the main contributing factors are fibre orientation and the number of fibre ends within the weldline region, both of which increase with increasing fibre concentration.

The overall dependence of weldline strength on volume fraction of glass fibres may be expressed as

$$\begin{aligned} \sigma_{cw} &\approx \sigma_{mw} \qquad (\phi_f \leqslant 0.044) \\ \sigma_{cw} &= \sigma_{mw} - \chi\phi_f \quad (\phi_f \geqslant 0.044) \end{aligned} \tag{19}$$

where σ_{cw} and σ_{mw} are the weldline strengths of the composite and the matrix, respectively. Both of these parameters increase with increasing rate as shown in Fig. 17a because of the brittleness of the matrix at higher rates. The value of χ is found to be much greater than one and increased with increasing rate ($\chi = 89.43$, 100.54 and 110.34 at cross-head speeds of 0.5 mm min^{-1}, 5 mm min^{-1} and 50 mm min^{-1}, respectively). A more useful way of rewriting Equation 19 for $\phi_f \geqslant 0.044$ is

$$\sigma_{cw} = \sigma_{mw}(1 - \psi\phi_f) \tag{20}$$

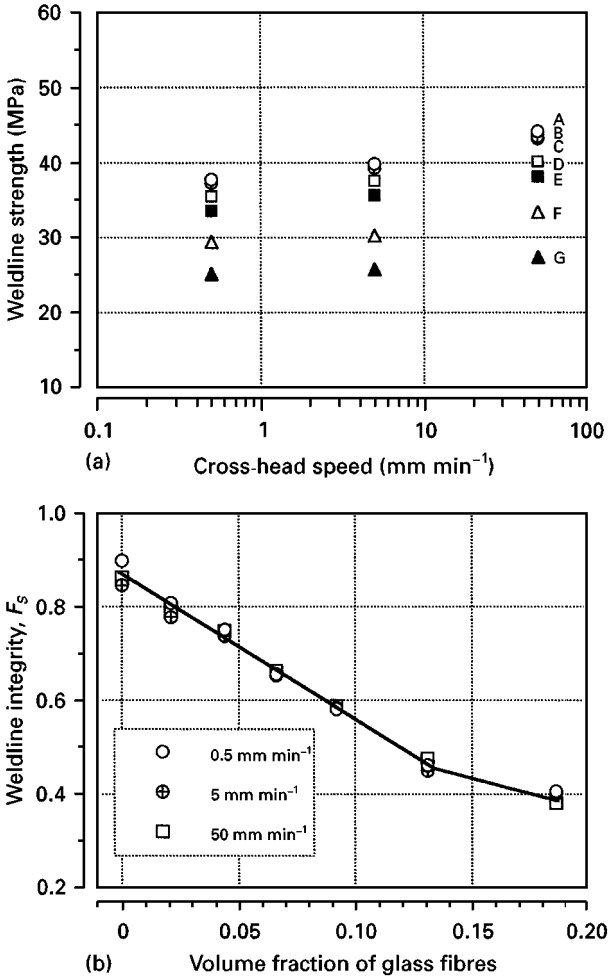

Figure 17 (a) Weldline strength versus loading rate for ASA and its composites. (b) Weldline integrity parameter for strength versus volume fraction of glass fibres.

where, for the range of cross-head speeds employed here, ψ is almost constant with an average value of 2.24 and standard deviation of 0.08.

Fig. 17b illustrates the effects of fibre concentration and loading rate on weldline integrity parameter for strengths (defined as weldline strength divided by the weld-free strength). It can be seen that the variation in weldline integrity factor resulting from different cross-head speeds is generally not very significant. However, data indicate that the weldline integrity is strongly influenced by the concentration of fibres in the specimen. In the concentration range between 0 and 13 vol%, the dependence of the weldline integrity factor for strength on ϕ_f can be reasonably expressed as

$$F_c = F_m(1 - \Omega\phi_f) \tag{21}$$

where F_c and F_m are the weldline integrity parameters for the composite strength and the matrix strength, respectively. The line drawn in Fig. 17b gives average F_m and Ω values of 0.867 and 3.55, respectively.

10.4. Work of fracture

Fig. 18a shows the dependence of the work of fracture on the volume fraction of the glass fibres for both welded and unwelded tensile specimens.

It can be seen from Fig. 18a that, for the case in which the fibre concentration is less than 5 vol%, work of fracture of the weld-free specimens decreases quite sharply with increasing ϕ_f. However, above this value and up to the concentration value of 13 vol%, very little variation, if any, in work of fracture was found with increasing ϕ_f. A further increase in fibre concentration led to a drop in the work of fracture for the reasons discussed earlier. It may be deduced also that the work of fracture is rate dependent; increasing with increasing rate.

Comparison of Fig. 18a and b clearly demonstrate that the presence of the weldline reduces the work of fracture of both filled and unfilled ASA specimens. This is attributed to the reduction in both the strength and the extension to failure of the specimen across the weldline. Although the severity of the energy loss due to the presence of the weldline was greatest for the unfilled ASA, a considerable reduction was also found for the reinforced materials, where the work of fracture was strongly dependent upon the concentration of the fibre, decreasing with increasing fibre concentration. It can be seen that the work of fracture of the weldline specimens is also affected by the rate of testing, increasing with increasing rate. However, the rate effect becomes increasingly less pronounced as the volume fraction of the fibres in the specimen is increased.

The extent to which the work of fracture had deteriorated in the presence of the weldline is clearly demonstrated in Fig. 18c through the weldline integrity parameter, F_u. It is seen that, in the case of the matrix, F_u has a value of 0.09 which then rises quite sharply, reaching a maximum value of 0.6 for reinforced grades containing 3–5 vol% glass fibres. Thereafter, F_u decreases with increasing ϕ_f, tending towards a limiting value of just below 0.2. It can be deduced also that the variation of F_u with ϕ_f is very much independent on the rate at which specimens are pulled.

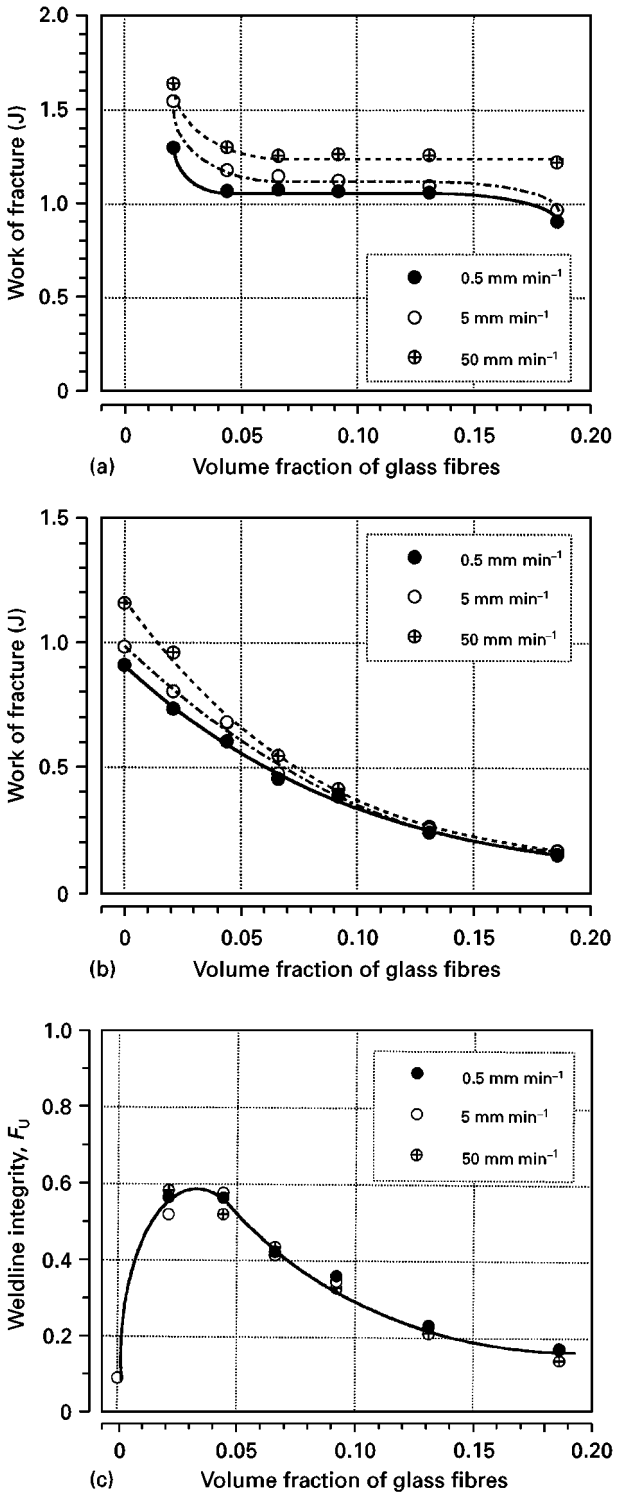

Figure 18 (a) Work of fracture versus volume fraction of glass fibres for unwelded specimens. (b) Work of fracture versus volume fraction of glass fibres for specimens with weldlines. (c) Weldline integrity parameter for work of fracture versus volume fraction of glass fibres.

10.5. Storage modulus

Fig. 19 compares values of the storage modulus and the flexural modulus as functions of fibre concentration. Seemingly, the agreement between the two moduli is reasonably good and the dependence of the storage modulus on ϕ_f may also by expressed by the rule of mixtures for moduli as given by Equation 10. The best linear regression line through the data (solid line in Fig. 19) gave E_m and λ_E values of 1.80 GPa and 0.48, respectively.

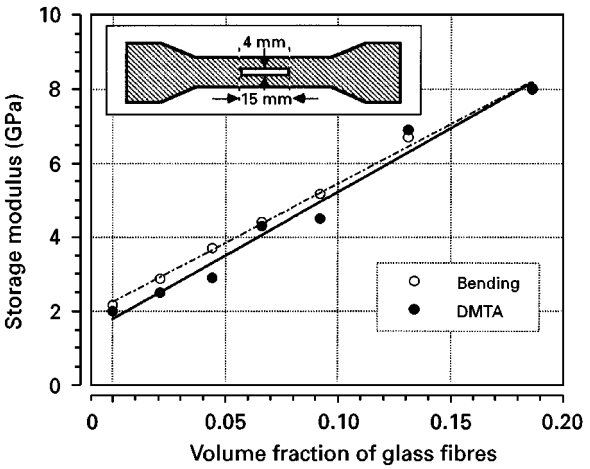

Figure 19 Comparison between the storage modulus and the flexural modulus as a function of volume fraction of glass fibres.

10.6. Impact strength

Fig. 20a shows the variation in the notched and the unnotched impact strengths as functions of ϕ_f. Since the unnotched specimens of the polymer matrix did not break under the testing conditions used here, it was not possible to measure its impact strength value. There is nevertheless, a clear indication that the addition of glass fibres to ASA polymer reduces the impact strength of both types of specimen. The dependence of both the notched and the unnotched impact strength on ϕ_f in many ways is similar to that observed for the work of fracture of unwelded specimens tested in tension (see Fig. 18a). The effect due to the notch alone on the impact strength is demonstrated in Fig. 20b through a notch integrity parameter, F_N, defined as the ratio of the two impact strengths (notched strength to unnotched strength). The general trend is that of increasing F_N with increasing ϕ_f, thus indicating that the sensitivity of notches upon impact strength becomes increasingly less severe as volume fraction of the glass fibres is increased.

10.7. Fracture toughness

The nature of the SENB load–displacement diagram for the glass-filled ASA materials is typified by the traces in Fig. 10. They show that, at maximum load, filled ASA specimens fracture in an unstable manner, particularly for the cases in which the length of the initial notch is less than $0.5W$. However, for a/W greater than 0.5, the nature of failure is by slow crack growth from the notch tip. As for unfilled ASA, our previous study [14] showed that the fracture behaviour of this material is ductile with slow crack propagation from the notch tip.

Linear elastic fracture analysis was used to evaluate the fracture toughness, K_m, corresponding to the maximum load. To evaluate K_m, the following equation was used [15] :

$$\sigma_m = \frac{K_m}{Ya^{1/2}} \tag{22}$$

where a is the initial crack length, σ_m is the maximum gross bending stress (equal to $3P_mS/2BD^2$) and Y is the finite width correction factor [15]. Fig. 21 shows the variation in σ_m as a function of $1/Ya^{1/2}$ for both ASA and its glass-filled composites, at cross-head displacement rates of 5 and 50 mm min^{-1}. Evidently, variation is reasonably linear and therefore independent of crack length for all materials studied here, as is the case for materials obeying linear elastic fracture mechanics. Clearly, data for ASA and its composites fall on one straight line, thus implying that the addition of glass fibres and their concentrations does not affect K_m (given by the slope of the line). This further supports the view that the adhesion between the fibres and the ASA material is poor.

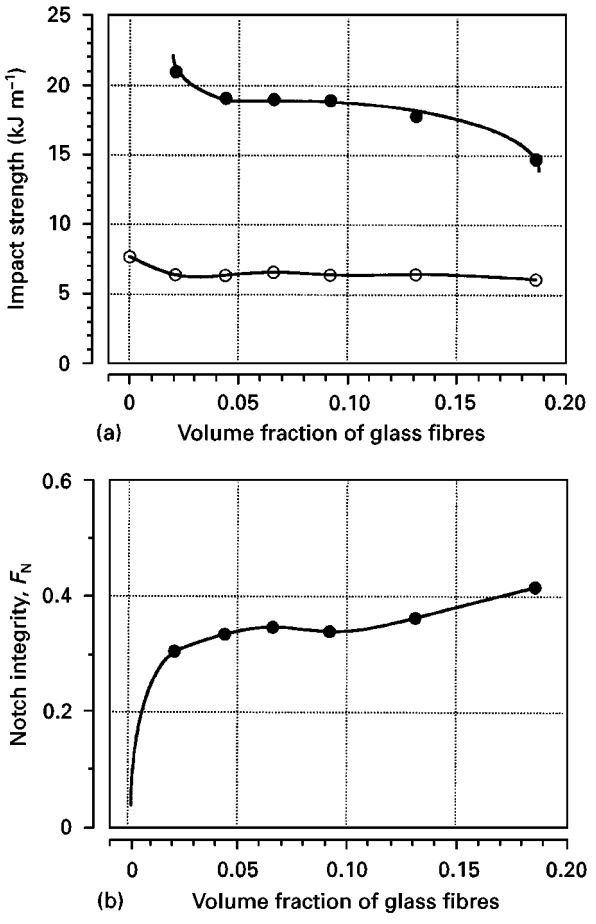

Figure 20 (a) Impact strength versus volume fraction of glass fibres. (●), unnotched; (○), notched. (b) Notched sensitivity parameter versus volume fraction of glass fibres.

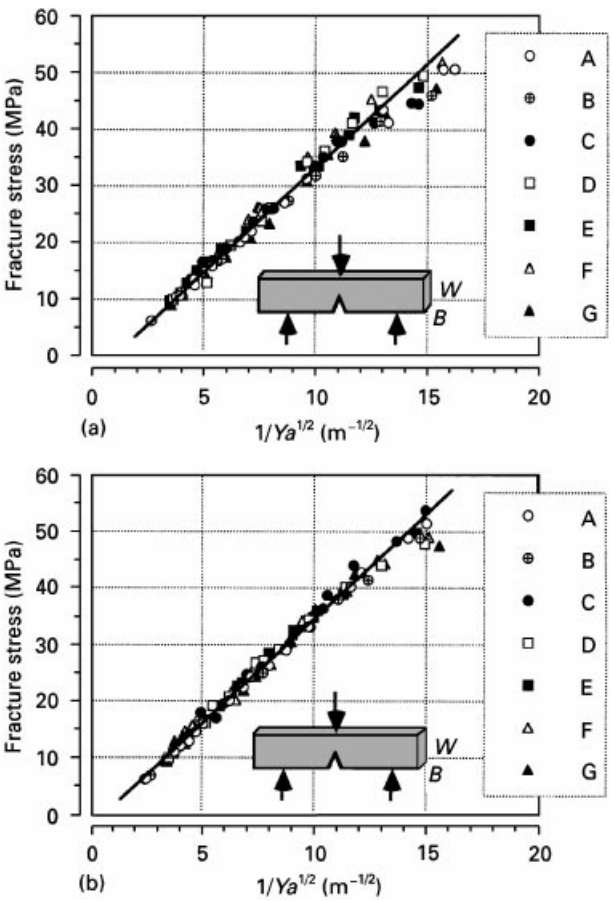

Figure 21 Fracture stress versus $1/Ya^{1/2}$ for ASA and its composites: (a) 5 mm min^{-1}; (b) 50 mm min^{-1}.

TABLE III Summary of the fracture data at cross-head displacement rates of 5 and 50 mm min^{-1}

ϕ_f (vol %)	Fracture data at 5 mm min^{-1}		Fracture data at 50 mm min^{-1}	
	K_m (MPa m$^{1/2}$)	G_m (kJ m^{-2})	K_m (MPa m$^{1/2}$)	G_m (kJ m^{-2})
0	3.16	4.62	3.36	5.23
2.1	3.11	3.36	3.32	3.83
4.4	3.32	2.97	3.52	3.34
6.6	3.40	2.62	3.43	2.67
9.2	3.36	2.18	3.45	2.30
13.1	3.48	1.81	3.42	1.75
18.6	3.11	1.21	3.44	1.47

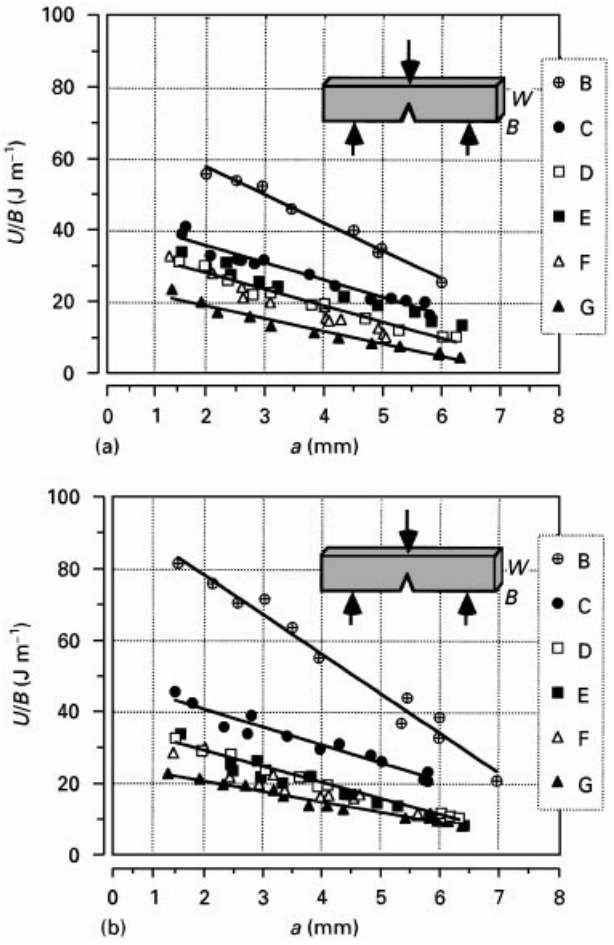

Figure 22 Total work of fracture per unit thickness versus crack length for filled ASA materials: (a) 5 mm min^{-1}; (b) 50 mm min^{-1}.

Considering that the average values of K_m at cross-head displacement rates of 5 mm min^{-1} and 50 mm min^{-1} are 3.28 ± 0.15 MPa m$^{1/2}$ and 3.42 ± 0.07 MPam$^{1/2}$, respectively, it may be inferred that K_m is not affected significantly by the rate of testing.

From the values of K_m given in Table III, values of the strain energy release rate, G_m, were evaluated from the relationship

$$G_m = \frac{K_m^2}{E} \tag{23}$$

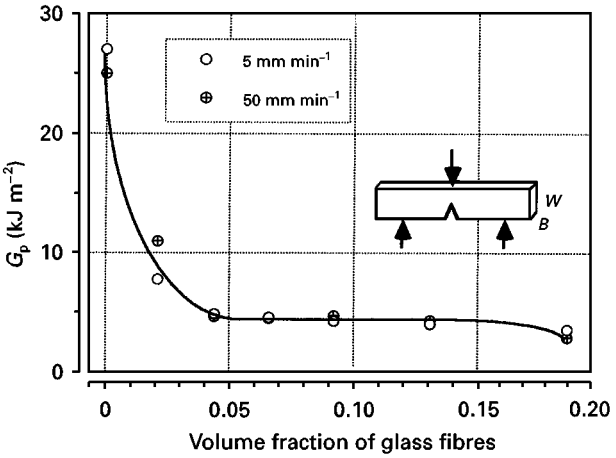

Figure 23 Crack propagation resistance versus volume fraction of glass fibres at cross-head displacement rates of 5 and 50 mm min^{-1}.

where E is the flexural modulus. Based on the values given in Table III, one can deduce that G_m decreases quite considerably with increasing ϕ_f. Undoubtedly, this is due to increasing stiffness of specimens with increasing ϕ_f.

From the total area under the load–displacement curves, values of the crack growth resistance, G_p, for the polymer and its composites were determined, using the generalized locus method [16]. According to this method, the resistance, G_p, to steady crack propagation can be determined from the following relationship:

$$G_p = \frac{1}{B}\frac{dU}{da} \tag{24}$$

where U represents the energy required for crack propagation, given by the total area enclosed by the loading curve and the x axis. If G_p is constant for a given specimen thickness, then the plot of U/B against crack length, a, should yield a linear fit. The slope of this linear fit represents G_p. Fig. 22 shows plots of U/B for the glass-filled composites as a function of crack length at cross-head displacement rates of 5 and 50 mm min^{-1}. It is evident that plots are reasonably linear with various slopes, G_p. These values are plotted in Fig. 23 as a function of ϕ_f, where it can be seen that the trend is very similar to that of the work of fracture in the tensile test (see Fig. 18a) or the impact strength (see Fig. 20).

11. Conclusions

The dependence of various mechanical properties on the volume fraction of reinforcing glass fibres in ASA copolymer was investigated. Results indicated that the addition of glass fibres has the following effects.

1. It enhances the ultimate tensile and flexural strengths of the polymer matrix. Variation for both strengths was reasonably linear with respect to ϕ_f and thus obeys the rule of mixtures for strengths. It was found that the strengths were greater in flexure than in tension. Moreover, the tensile strength values of both

unfilled and filled ASA were considerably reduced in the presence of the weldline. The weldline integrity parameter for the resin was approximately 0.87 and for the composite containing 19 vol% glass fibres was as low as 0.2. Both strengths were found to be dependent on the rate of testing, increasing with increasing testing rate.

2. It enhances the elastic modulus of the polymer matrix. The elastic modulus was not affected by the loading mode and was found to be a linear function of ϕ_f which was subsequently described by the rule of mixtures. This quantity for both filled and unfilled ASA was not affected by the weldline. The weldline integrity parameter for the modulus ranged between 1.0 and 0.95.

3. It reduces the elongation to yield and to break as well as the total work of fracture of the polymer matrix. These quantities were reduced in the presence of the weldline. The weldline integrity parameter for the matrix was approximately 0.09 and for the composites it ranged between 0.6 and 0.2 depending on the concentration of the fibres.

4. It reduces both the notched and the unnotched impact strength of the matrix.

5. It has little effect, if any, on the fracture toughness of the polymer matrix. This was attributed to the poor adhesion between the fibre and the matrix. The strain energy release rate value for the polymer matrix was found to be higher than those of its composites.

Acknowledgement

The authors gratefully acknowledge the support provided by BASF in providing the materials.

References

1 A. KELLY and W. R. TYSON, *J. Mech. Phys. Solids.* **6** (1965) 13.
2 K. J. DIN and S. HASHEMI, *J. Mater. Sci.* **32** (1997) 375.
3 M. R. PIGGOTT, M. KO and H. Y. CHUANG, *Compos. Sci. Technol.* **48** (1993) 291.
4 G. KALAPRASAD, K. JOSEPH and S. THOMAS, *J. Mater. Sci.* **32** (1997) 4261.
5 M. R. PIGGOTT, *J. Compos. Mater.* **28** (1994) 588.
6 S. HASHEMI, M. T. GILBRIDE and J. M. HODGKINSON, *J. Mater. Sci.* **31** (1996) 5017.
7 A. CHRYSOSTOMOU and S. HASHEMI *J. Mater. Sci.*, **33** (1998) 1165.
8 D. HULL, "Introduction to composite materials" (Cambridge University Press, Cambridge, Cambridgeshire, 1981).
9 J. KARGER-KOCSIS and K. FRIEDRICH, *Polymer* **27** (1986) 1753.
10 M. FOLKES, "Short fibre reinforced thermoplastics" (Rsch Studies Press, Wiley, New York, 1982).
11 D. C. LEACH and D. R. MOORE, *Composites* **16** (1985) 113.
12 B. PUKANSZKY, *ibid.* **21** (1990) 255.
13 W. WEIBULL, *J. Appl. Mech.* **18** (1951) 293.
14 Z. U. NABI and S. HASHEMI, *J. Mater. Sci.* **31** (1996) 5593.
15 W. F. BROWN and J. E. SRAWLEY, ASTM Special Technical Publication 410 (American Society for Testing and Materials, Philadelphia, Pennsylvania, 1996).
16 B. H. KIM and C. R. JOE, *Polym. Testing* **7** (1987) 355.

Received 4 November 1997
and accepted 3 March 1998